J. Fluid Mech. (1994), *vol.* 278, *pp.* 63–81

Expulsion of particles from a buoyant blob in a fluidized bed

By G. K. BATCHELOR[1] AND J. M. NITSCHE[2]

[1] Department of Applied Mathematics and Theoretical Physics, University of Cambridge, Silver Street, Cambridge CB3 9EW, UK

[2] Department of Chemical Engineering, State University of New York, Buffalo, NY 14260, USA

(Received 3 September 1993 and in revised form 20 May 1994)

It is a significant feature of most gas-fluidized beds that they contain rising 'bubbles' of almost clear gas. The purpose of this paper is to account plausibly for this remarkable property first by supposing that primary and secondary instabilities of the fluidized bed generate compact regions of above-average or below-average particle concentration, and second by invoking a mechanism for the expulsion of particles from a buoyant compact blob of smaller particle concentration. We postulate that the rising of such an incipient bubble generates a toroidal circulation of the gas in the bubble, roughly like that in a drop of liquid rising through a second liquid of larger density, and that particles in the blob carried round by the fluid move on trajectories which ultimately cross the bubble boundary. Numerical calculations of particle trajectories for practical values of the relevant parameters show that a large percentage of particles, of such small concentration that they move independently, are expelled from a bubble in the time taken by it to rise through a distance of several bubble diameters.

Similar calculations for a liquid-fluidized bed show that the expulsion mechanism is much weaker, as a consequence of the larger density and viscosity of a liquid, which is consistent with the absence of observations of relatively empty bubbles in liquid-fluidized beds.

It is found to be possible, with the help of the Richardson–Zaki correlation, to adjust the results of these calculations so as to allow approximately for the effect of interaction of particles in a bubble in either a gas- or a liquid-fluidized bed. The interaction of particles at volume fractions of 20 or 30% lengthens the expulsion times, although without changing the qualitative conclusions.

1. Introduction

Compact regions of low particle concentration may be observed to rise through a gas-fluidized bed when the gas velocity is sufficiently large. These buoyant 'bubbles' have steady shapes resembling gas bubbles rising through liquid, as may be seen from many published photographs. The bubbles may be formed by discharging gas from an orifice in the interior of the fluidized bed, or they may be a consequence of non-uniformity of the porosity of the base plate. There is a common belief among chemical engineers that bubbles may also form spontaneously in the interior of a gas-fluidized bed.

It is generally agreed that the amplitude of vertically propagating plane-wave disturbances to a statistically uniform bed with particle volume fraction between 0.4 and 0.5 may grow exponentially under certain conditions (see for example Batchelor

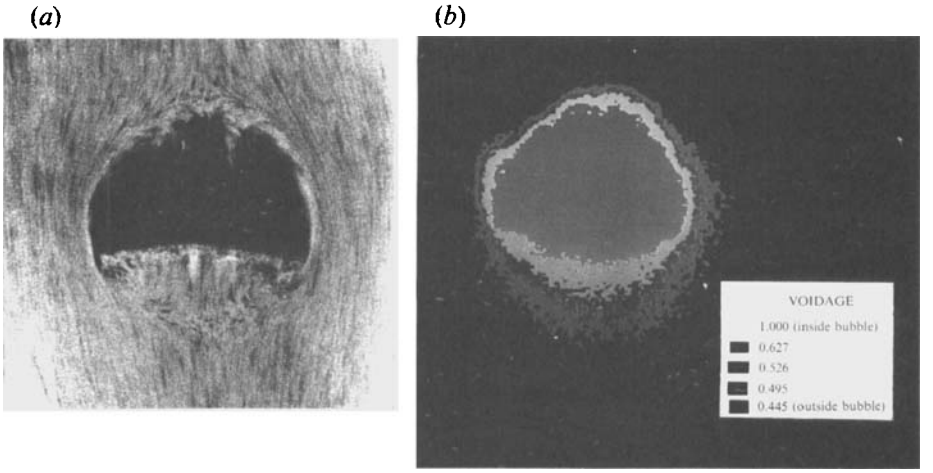

FIGURE 1. (*a*) Photograph of a blown half-bubble rising through a gas-fluidized bed against a nearly vertical glass plate, taken by a camera moving with the bubble. (From Reuter 1963.) (*b*) X-ray image showing the variation of particle concentration in a transition layer at the bubble surface. The bands correspond to different values of the concentration, and the value in the interior of the bubble is effectively zero. (From Yates, Cheesman & Sergeev 1994.)

1988). There is then the possibility of a secondary instability which overturns alternate horizontal layers in which the vertical gradient of particle concentration is positive (Batchelor 1993). Compact regions of below-average or above-average concentration with linear dimensions related to the wavelengths of the fastest-growing disturbances in the primary and secondary instabilities may thus be generated, and the thesis to be adopted here is that the buoyant compact regions of below-average concentration become visible bubbles.

A prominent and persistent feature of observed bubbles in gas-fluidized beds, regardless of the method of their formation, is that the concentration of particles inside a bubble is small. This may be inferred from the fact that the observed speed with which a bubble rises relative to the particles is approximately $1.0\,(gR)^{1/2}$, where R is the radius of the sphere having the same volume as the bubble, which is close to the speed of a large gas bubble rising through liquid. (For data about bubbles in fluidized beds and theories devised to account for some of the data, see Davidson & Harrison 1963 and the useful review article by Davidson, Harrison & Guedes de Carvalho 1977.) Direct examination of a bubble in a fluidized bed gives an impression of relative emptiness of the interior. In the case of blown half-bubbles rising in a fluidized bed against a nearly vertical glass plate, like that shown in figure 1 (*a*), the emptiness is often evident. Recent observations of particle concentration in and near a blown bubble in a gas-fluidized bed using X-rays have revealed clearly a layer surrounding the bubble in which the concentration varies rapidly from a value near the maximum for fluidization at the outer boundary to a value near zero at the inner boundary (see figure 1 *b*).

It seems very unlikely that an instability of the initially uniform distribution of particle concentration in a gas-fluidized bed could cause such a complete separation of particles and fluid as to produce compact regions in which the particle concentration is relatively small. Some further separation process seems to be needed, and one of us has speculated that this additional process is an expulsion of particles from the interior of a bubble by the centrifugal force on a particle trying to follow the circulating motion

of the gas inside the rising buoyant blob (Batchelor 1991). The purpose of the present paper is to test this speculation by determining numerically the rate at which small particles in the interior of a rising buoyant blob move outward across the blob boundary as a consequence of gravity and inertia forces acting on the particle. Investigations of the trajectories of small particles moving in a given fluid flow field are not uncommon (see, for example, Maxey & Corrsin 1986), and are usually concerned with the trapping of particles within certain portions of the flow field. In our case the opposite process of expulsion of particles from a buoyant blob in a fluidized bed is of interest. The conditions we shall assume make it almost self-evident that expulsion of particles from a rising buoyant blob in a gas-fluidized bed does occur, but we believe the quantitative aspects of the particle trajectories have some value.

Empty bubbles in liquid-fluidized beds appear not to have been observed, even though a uniform liquid-fluidized bed may be unstable. In §5 we consider whether the proposed expulsion process operates in the case of a liquid-fluidized bed.

We note some early related work by Davidson & Harrison (1963, chap. 5) who address the following question: what are the conditions under which an empty bubble will be destroyed by their postulated process of entrainment of particles into the bubble? Our objective on the other hand is to clarify the process of formation of an empty bubble, beginning with a compact region of below-average concentration of particles. The general conclusions of the two investigations appear to be compatible, although the mechanisms concerned are essentially different and are relevant to different parameter ranges. The parameter values that we are concerned with (e.g. those represented in figure 8) are such that the minimum fluid velocity for fluidization, estimated using equation (2.4), is small by comparison with the bubble rise speed, indicating that the wake-entrainment effects considered by Davidson & Harrison (1963) are small for bubbles of the kind considered here.

2. The relevant particle and fluid properties for a gas-fluidized bed

It is desirable to take note of representative properties of the particles and fluids used in gas-fluidized beds in industry and the laboratory so that we can see which mechanical processes are relevant. The shape of the particles is not very important, provided they are compact, and we shall suppose them to be solid spheres. The densities are normally of order unity, and it is convenient to take the particle density ρ_p as 1.00 g cm^{-3}, or sometimes as an integral multiple thereof, when a numerical value is needed. The fluidizing fluid will be assumed to be air at 20 °C and 1 atmosphere, with density $\rho_f = 1.205 \times 10^{-3}$ g cm^{-3} and viscosity $\mu = 1.81 \times 10^{-4}$ g cm^{-1} s^{-1}. Guided by published photographs of bubbles in gas-fluidized beds, we take 2 cm as a typical value of the radius R of a sphere of the same volume as a bubble.

Values of the particle radius a between 30 μm and 300 μm are common in fluidized beds. We shall require an expression for the drag force exerted by the fluid on an isolated spherical particle moving with steady speed V_0 relative to axes fixed in the fluid far from the particle, and in order to embrace this range of values of a and the corresponding values of V_0 for particles falling under gravity the expression for the drag must be valid for both small and large values of the particle Reynolds number

$$\mathbb{R}_0 = 2a\rho_f V_0/\mu. \tag{2.1}$$

We shall write the drag force on such an isolated particle as

$$6\pi a\mu V_0 D_{V_0} \tag{2.2}$$

where D_{V_0} is a non-dimensional drag coefficient given empirically by

$$D_{V_0} = (1+0.13\mathbb{R}_0^{1/2})^2 \tag{2.3}$$

according to Foscolo & Gibilaro (1984).

An expression for the mean velocity of the particles in a statistically homogeneous dispersion moving under the action of a common force – as in parts of the fluidized bed away from bubbles – is also relevant. We shall make use of the empirical relation due to Richardson & Zaki (1954), namely

$$V_\phi = V_0(1-\phi)^n, \tag{2.4}$$

where V_ϕ is the mean velocity of particles with volume fraction ϕ, relative to the mean volume-flux velocity of the fluid, and n varies monotonically with the Reynolds number (2.1) from 4.65 at $\mathbb{R}_0 \to 0$ to 2.39 at $\mathbb{R}_0 \to \infty$. The strong dependence of V_ϕ on ϕ here is a consequence of the hydrodynamic interaction of particles.

Now the gas within a buoyant blob rising through the fluidized bed with speed W relative to the particles in the bed is set into motion by the rising of the blob. We suppose for the moment that the blob is effectively empty of particles, in which event W is known empirically to be about $1.0\,(gR)^{1/2}$. According to our simple model of a buoyant blob, the blob is spherical, the interior gas motion is driven by the tangential stress at the blob boundary exerted by the particles and fluid streaming around the rising blob, and is axisymmetric, with closed nested streamlines like those in a toroidal vortex. Real bubbles in a gas-fluidized bed have an internal circulation with closed fluid streamlines which extend a little beyond the visible bubble boundary into a 'cloud', but we shall suppose the penetration distance to be negligibly small. It is natural also to suppose that the magnitude of the interior gas velocity is comparable with that of the exterior streaming motion (velocities being relative to the blob in both cases). An important consequence of this assumption is that the centrifugal force on a particle carried round by the fluid inside a spherical bubble is of the same order of magnitude as gravity.

We shall suppose for convenience in the later numerical calculations that the velocity of the fluid inside a spherical bubble of radius R and relative to it is represented by the simple stream function

$$\Psi_f = \tfrac{1}{2}u_0 r^2 \sin^2\theta\left(\frac{R^2-r^2}{R^2}\right) \quad (r \leqslant R), \tag{2.5}$$

where the origin of the spherical polar coordinate system is fixed at the bubble centre and the constant u_0 is the fluid speed at the centre of the sphere. The corresponding streamlines are shown in figure 2. This interior velocity distribution is actually the same as that in two well-known flow fields with a spherical boundary, namely a small drop of viscous liquid rising under gravity in a second fluid of different density and viscosity, and a Hill's spherical vortex (Batchelor 1967). However, that coincidence is of no significance here. The flow field (2.5) is not intended to represent accurately the gas flow in the interior of a real bubble in a fluidized bed. Our intention is simply to show that rapid particle expulsion can occur when the interior gas flow is primarily toroidal with a velocity of certain magnitude.

As already stated we suppose that the rise speed of the blob, W, may be equated in order of magnitude with a velocity representative of the interior fluid motion, and for simplicity we take

$$u_0 \approx W \approx (gR)^{1/2}. \tag{2.6}$$

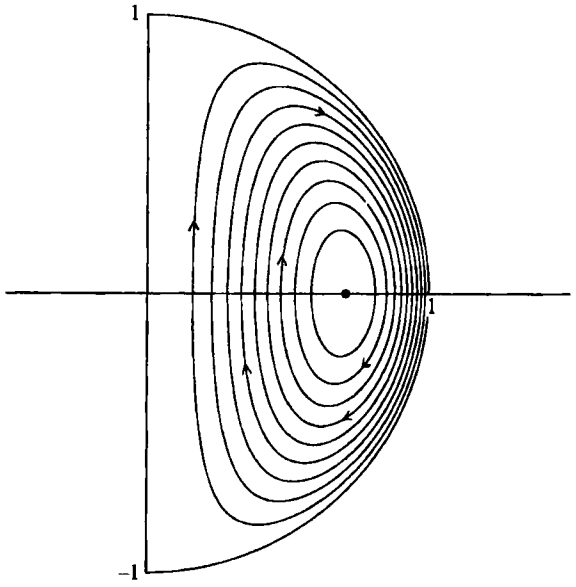

FIGURE 2. Streamlines of the assumed steady flow of fluid within the bubble.

Finally there is the question: what value of the concentration of particles in the interior of the buoyant blob should be assumed? It is known that there are effects of hydrodynamic interaction of the particles in a homogeneous dispersion which are significant when the particle volume fraction ϕ exceeds a few percent. We should like to be able to show whether the particles in a compact region of a fluidized bed in which the concentration is smaller than that in the remainder of the bed are expelled by inertia forces on the particles. The compact regions of smaller concentration are believed to be the end product of primary and secondary instabilities of an initially uniform bed (Batchelor 1991), but no information about the fluctuations in particle concentration brought about by nonlinear processes in the last stages of instabilities is available. One might guess that, in an initially uniform bed for which $\phi = 0.4$ say, positive and negative fluctuations in the particle concentration of magnitude between 25 and 50% of the overall mean are generated in this way. If so, buoyant blobs in which ϕ initially lies between 0.2 and 0.3 are to be expected and it is desirable to include the effects of hydrodynamic interaction of particles in an accurate analysis of particle expulsion from the blob.

However, taking account of hydrodynamic interaction is difficult enough in the relatively simple case of statistical homogeneity of the particle positions and motions, and is not within our capabilities in the more complicated geometry of a buoyant blob. We propose therefore to assume initially that the particle concentration within the buoyant blob is sufficiently small for the particles to move independently of each other. This should be permissible when the particle volume fraction is less than a few percent, as it is in the final stages of an expulsion process. Later in §6 we shall put forward a hypothesis using (2.4) from which the effect of particle interactions on the rate of expulsion of particles at larger concentrations may be estimated roughly.

Here are the specific values and assumptions on which our calculations of the trajectories of particles in a buoyant blob in a gas-fluidized bed will be based:

(1) the values of ρ_f and μ are those for air at NTP;

(2) $\rho_p = 1\ \mathrm{g\ cm^{-3}}$ (or an integral multiple thereof);

(3) we adopt empirical relations between drag on a moving particle and (i) particle Reynolds number, namely (2.3), and (ii) particle concentration, namely (2.4);

(4) R (equivalent blob radius) = 2 cm;

(5) particle volume fraction within blob is so small that particles move independently;

(6) blob rise speed $W \approx 1.0(gR)^{1/2}$;

(7) fluid flow within an empty blob is given by (2.5), with $u_0 = W$.

3. The governing equation for a particle in a bubble in a gas-fluidized bed

A particle within a buoyant blob of fluid moves under the influence of gravity, its own inertia, and the viscous resistance exerted by the fluid. Hence, in accordance with the assumptions described in §2, and with neglect of all terms containing the fluid density as a factor, the equation of motion of a particle is

$$m\frac{\mathrm{d}\boldsymbol{v}}{\mathrm{d}t} = m\boldsymbol{g} - 6\pi\mu a(\boldsymbol{v}-\boldsymbol{u})\,D_{|\boldsymbol{v}-\boldsymbol{u}|}, \tag{3.1}$$

where m is the particle mass, $\boldsymbol{v}$ is the particle velocity, $\boldsymbol{u}$ is the ambient fluid velocity at the instantaneous position of the particle, and the non-dimensional drag force $D_{|\boldsymbol{v}-\boldsymbol{u}|}$ depends on the particle Reynolds number $2a\rho_f|\boldsymbol{v}-\boldsymbol{u}|/\mu$ in accordance with (2.3).

An important parameter of this equation (3.1) is the viscous relaxation time of a particle (that is, the time for the relative velocity of a particle acted on only by the viscous fluid resistance to relax exponentially back to zero), namely

$$\tau_0 = \frac{m}{6\pi\mu a} = \frac{2a^2\rho_p}{9\mu}. \tag{3.2}$$

Equation (3.1) can be rewritten in terms of τ_0 as

$$\frac{\mathrm{d}\boldsymbol{v}}{\mathrm{d}t} = \boldsymbol{g} - \frac{\boldsymbol{v}-\boldsymbol{u}}{\tau_0}D_{|\boldsymbol{v}-\boldsymbol{u}|}. \tag{3.3}$$

This is one of the basic equations of 'dusty-gas theory' (Marble 1970), and is normally used in the low-Reynolds-number form for which $D_{|\boldsymbol{v}-\boldsymbol{u}|} = 1$. In the calculations to be reported here, the dependence of the drag coefficient on $|\boldsymbol{v}-\boldsymbol{u}|$ is important.

The terms in (3.3) may be made dimensionless using R and u_0 as reference quantities, whence

$$\frac{\mathrm{d}\boldsymbol{V}}{\mathrm{d}T} = \frac{\boldsymbol{j}}{F} - \frac{\boldsymbol{V}-\boldsymbol{U}}{S}D_{|\boldsymbol{v}-\boldsymbol{u}|}, \tag{3.4}$$

where $\boldsymbol{j}$ is the unit vector in the downward vertical direction and

$$T = tu_0/R, \quad \boldsymbol{U} = \boldsymbol{u}/u_0, \quad \boldsymbol{V} = \boldsymbol{v}/u_0. \tag{3.5}$$

A particle trajectory thus depends on the two dimensionless parameters

$$S = \frac{\tau_0 u_0}{R} = \frac{2a^2u_0\rho_p}{9R\mu}, \quad F = \frac{u_0^2}{gR}, \tag{3.6}$$

S being the Stokes number and F the Froude number. However, since the representative fluid speed in the interior of the bubble (u_0) is being equated to the bubble rise speed W, which is empirically equal to $(gR)^{1/2}$, we see that F is approximately unity,

a (μm)	$\mathbb{R}_0$	$\mathbb{R}_1$	S
10	1.55×10^{-2}	5.90×10^{-1}	2.72×10^{-2}
20	1.17×10^{-1}	1.18×10^{0}	1.09×10^{-1}
30	3.71×10^{-1}	1.77×10^{0}	2.45×10^{-1}
40	8.20×10^{-1}	2.36×10^{0}	4.35×10^{-1}
50	1.49×10^{0}	2.95×10^{0}	6.80×10^{-1}
60	2.40×10^{0}	3.54×10^{0}	9.79×10^{-1}
70	3.54×10^{0}	4.13×10^{0}	1.33×10^{0}
80	4.94×10^{0}	4.72×10^{0}	1.74×10^{0}
90	6.57×10^{0}	5.31×10^{0}	2.20×10^{0}
100	8.44×10^{0}	5.90×10^{0}	2.72×10^{0}
150	2.12×10^{1}	8.85×10^{0}	6.12×10^{0}
200	3.90×10^{1}	1.18×10^{1}	1.09×10^{1}
250	6.14×10^{1}	1.47×10^{1}	1.70×10^{1}
300	8.78×10^{1}	1.77×10^{1}	2.45×10^{1}

TABLE 1. Values of the dimensionless parameters assuming air at 20 °C and atmospheric pressure to be the suspending fluid, having density $\rho_f = 1.205 \times 10^{-3}$ g cm^{-3} and viscosity $\mu = 1.81 \times 10^{-4}$ g cm^{-1} s^{-1}. The particle density ρ_p is taken to be 1.0 g cm^{-3}.

corresponding to the near equality of inertial and gravitational forces on a particle. Thus S is the only variable parameter entering the governing equation explicitly. This is a distinguishing feature of a 'dusty-gas' flow system in which the fluid velocities are themselves generated by gravity. With the replacement of u_0 by $W = (gR)^{1/2}$, S can be written as

$$S = \frac{2a^2 g^{1/2} \rho_p}{9R^{1/2}\mu}. \tag{3.7}$$

The fluid velocity $\boldsymbol{u}$ in (3.1) is evaluated at the instantaneous position of the particle, and in general an equation of motion of the fluid which includes the force exerted on the fluid by particles should be introduced for the determination of $\boldsymbol{u}$. If the mean spacing of particles in the buoyant blob is small compared with the blob diameter, we may regard the viscous force exerted on the fluid by the particles as equivalent to a distributed body force per unit volume equal to

$$\phi \rho_p \frac{\boldsymbol{v}-\boldsymbol{u}}{\tau_0} D_{|\boldsymbol{v}-\boldsymbol{u}|} = \frac{\rho_f u_0^2}{R} \frac{N}{S} (\boldsymbol{V}-\boldsymbol{U}) D_{|\boldsymbol{v}-\boldsymbol{u}|},$$

where $N = \phi \rho_p / \rho_f$ is the particle mass loading (that is, the fraction of the total mass of the mixture contributed by the particles). Since $|\boldsymbol{V}-\boldsymbol{U}| D_{|\boldsymbol{v}-\boldsymbol{u}|}$ is in general of order unity, we see that the ratio of this body force to the fluid inertia force (of magnitude $\rho_f u_0^2/R$) is N/S. Hence if $N/S \ll 1$ the fluid motion is not appreciably affected by the presence of the particles, and may be regarded as a given consequence of some external factor (which in our case is the tangential stress at the blob boundary associated with the rising of the buoyant blob under gravity). Now with $\rho_p = 1$ g cm^{-3} and the values of ρ_f and μ proposed in §2, and ϕ chosen as 0.01 in keeping with our neglect of hydrodynamic interactions of particles, we have $N = 8.3$. The ratio N/S is then equal to 0.76 when $a = 200$ μm (a relatively large value) and $R = 2$ cm, and is proportional to a^{-2} (for given ϕ); on the other hand when a is small the particles tend to move with the fluid and $|\boldsymbol{V}-\boldsymbol{U}| = O(a^2)$. It appears therefore that the presence of particles in the middle of the size range may have some effect on the fluid flow field. However, the order-of-magnitude estimate (2.6) is still likely to hold, and we shall regard the fluid

flow field in the buoyant blob as given, and as being described by (2.5), the penalty being that our results may be strictly applicable only to very small concentrations of particles in the buoyant blob.

The final preparation for the numerical calculation of particle trajectories is the construction of table 1 giving values of the Reynolds number $\mathbb{R}_0$ and the Stokes number S as functions of the particle radius a on the basis of the assumptions listed at the end of §2. It is convenient to include values of $2au_0\rho_f/\mu (\equiv \mathbb{R}_1)$ because the Reynolds number of the flow about a particle moving with velocity $\boldsymbol{v}-\boldsymbol{u}$ relative to the fluid locally is needed for substitution in (2.3) and is

$$\mathbb{R}_{|\boldsymbol{v}-\boldsymbol{u}|} = \frac{2a|\boldsymbol{v}-\boldsymbol{u}|\rho_f}{\mu} = \mathbb{R}_1|\boldsymbol{V}-\boldsymbol{U}|. \tag{3.8}$$

This Reynolds number $\mathbb{R}_{|\boldsymbol{v}-\boldsymbol{u}|}$ determines the drag coefficient $D_{|\boldsymbol{v}-\boldsymbol{u}|}$, and so $\mathbb{R}_1$ is a second governing parameter, additional to but less important than S.

4. Particle trajectories

Equation (3.4), expressed as a system of four coupled first-order ODEs for the radial (σ) and axial (z) coordinates of a particle and their time derivatives, may be solved numerically by fourth-order Runge–Kutta integration for the case of motion confined to a vertical plane through the bubble axis. (In the absence of an azimuthal force, any initial motion of a particle about the bubble axis would soon be damped out and could make no essential contribution to particle expulsion.) For definiteness, the initial particle velocity at the point of release is chosen so that the initial particle acceleration is zero. Dimensionless time steps of 0.01 are sufficiently small to allow the particle motion to be tracked accurately for even the smallest values of S considered. Figure 3 shows calculated trajectories for a number of particle radii ranging from 20 to 80 μm following release on the equatorial plane at evenly spaced values of the non-dimensional radial coordinate σ between 0 and 1. Small particles follow the fluid streamlines closely owing to the small effects of particle inertia and gravity relative to viscous drag. In the limit of vanishing particle radius $S \to 0$ and equation (3.4) formally reduces to $\boldsymbol{V} = \boldsymbol{U}$, and the trajectories coincide with the fluid streamlines shown in figure 2. The effect of inertia and gravity for $S \ll 1$ is to cause only small perturbations to this limiting motion, and small effects accumulate to produce a significant deviation from the fluid streamlines (and, in particular, expulsion) only after considerable time has elapsed. Outward spiralling and sedimentation relative to the fluid are of equal strength, since $F = 1$. Each rapidly becomes more pronounced with increasing particle size.

Several features of the trajectories merit discussion. First, owing to the directional bias imparted by gravity, expulsion takes place almost exclusively below the equatorial plane. Second, there is a hemispherical cap-shaped region at the top of the bubble whose thickness increases with a and which is devoid of particle path lines. Particles initially in the cap are expelled at an early stage, and are not replaced because particles moving up near the axis have insufficient upward inertia to overcome both viscous drag and gravity and re-enter the cap region. Third, there is manifested clearly in figure 3 a focusing of trajectories. This is to be expected, as there is an inherent discreteness associated with the expulsion process. In particular, there must exist critical values of the initial radial position coordinate (σ_0) at which the number of circuits made by a trajectory before exiting jumps by one. A particle may just fail to reach the bubble boundary and so makes one more circuit. Thus, the expulsion time T_{exit} does not vary

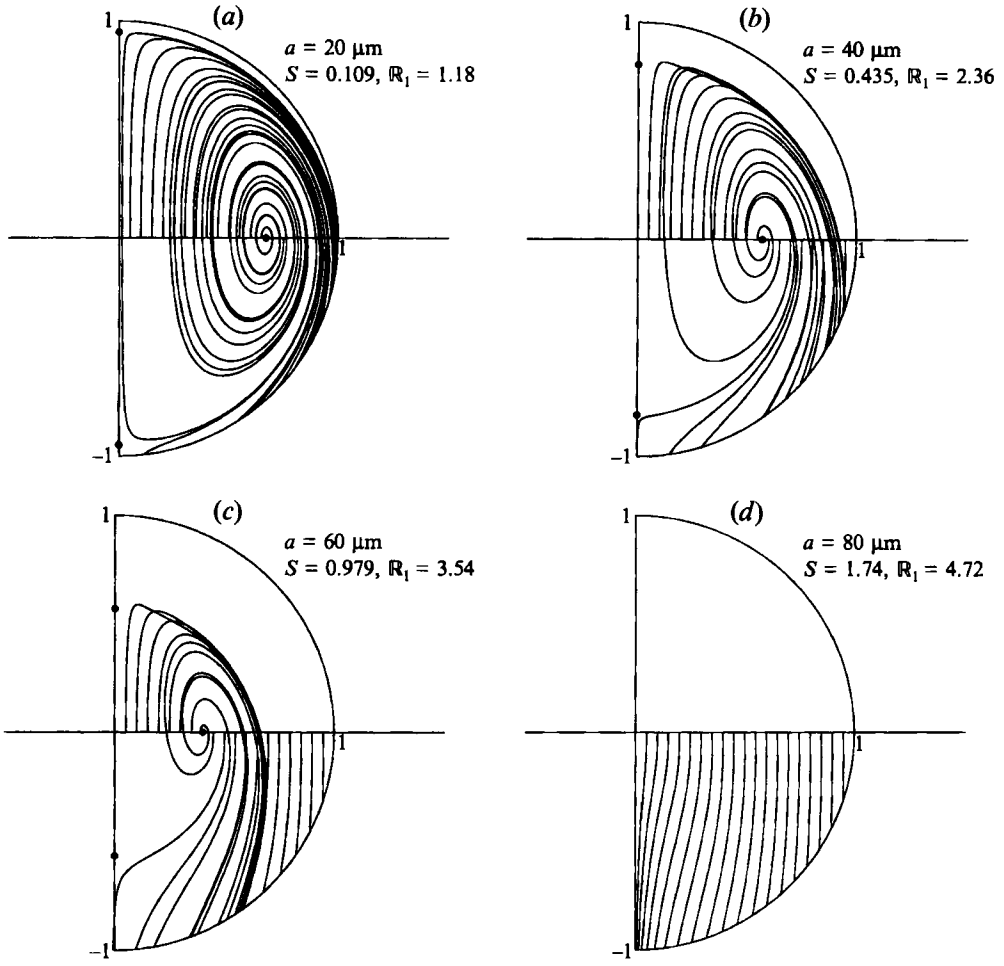

FIGURE 3. Trajectories (relative to the bubble) of particles of radius a released on a horizontal line through the centre of a rising spherical bubble in an air-fluidized bed. Darkened circles in (*a*), (*b*) and (*c*) indicate the three particle stagnation points.

continuously with σ_0, as may be seen in figure 4. This sensitivity of T_{exit} to initial conditions must be associated with a relative insensitivity of particle paths to values of σ_0 in the intervals between the critical values, whence the focusing of trajectories.

Other features of figures 3 and 4 are closely related to the existence of three particle stagnation points in a meridian plane (marked with darkened circles in figure 3*a–c*). At these points there is a balance between gravitational down-force and drag due to fluid up-flow, and a particle released there with zero velocity remains stationary. The particle stagnation point lying on the σ-axis is a centre of rotation (locally) which is displaced horizontally inwards by gravity from the eye of the toroidal vortex of the fluid flow. The closer is the point of particle release to this centre, the longer is the exit time, because the force on the particle causing it to spiral outwards goes to zero linearly with distance from the centre, giving the main spike in figure 4 at which T_{exit} diverges. The particle stagnation points on the z-axis have the character of saddle points. The critical values of σ_0 correspond to trajectories leading exactly to the lower particle stagnation point, like that in figure 5(*a*), for which the time dependence of the radial

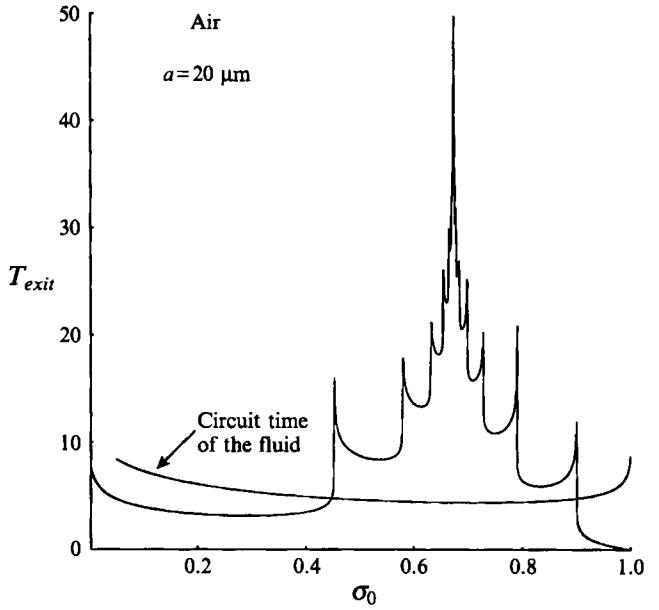

FIGURE 4. The expulsion time of a particle released at a horizontal distance σ_0 from the centre of the bubble in an air-fluidized bed. The time taken by a fluid particle in making one circuit of a closed streamline is shown for comparison. The sudden jumps in T_{exit} correspond to sudden changes in the number of circuits made by a particle before crossing the bubble boundary; compare figure 3(*a*).

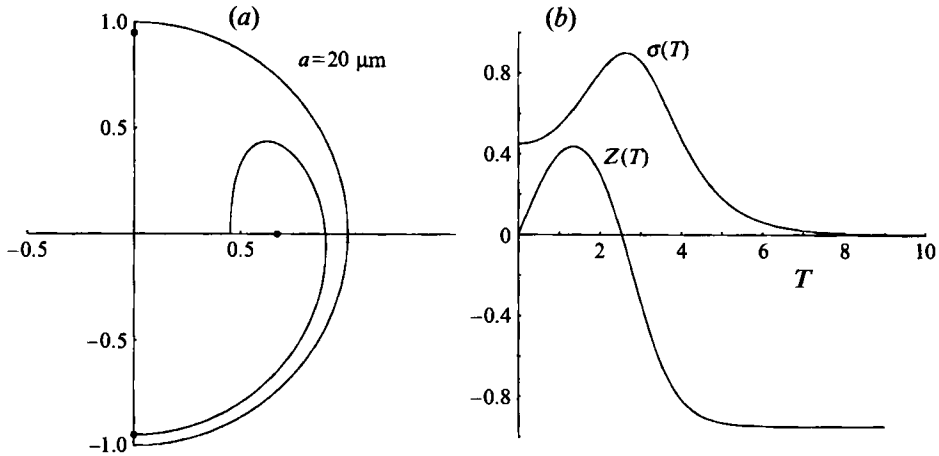

FIGURE 5. (*a*) One of the many trajectories that lead to the lower particle stagnation point on the z-axis, corresponding to the left-most spike in figure 4 at $\sigma_0 = 0.4518$. (*b*) The position coordinates of a particle on the trajectory shown in (*a*) as functions of T.

and axial coordinates σ, Z are shown in figure 5(*b*), and give rise to divergences of T_{exit} manifested as auxiliary spikes on both sides of the central spike in figure 4. As $S \to 1$ all three particle stagnation points move towards the bubble centre, and for $S > 1$ the drag arising from the fluid flow is everywhere weaker than the gravitational force, so that particle stagnation points disappear. Thus, for $S > 1$, all trajectories represent monotonic fall under gravity which is perturbed but nowhere dominated by the gas flow (cf. figure 3*d*).

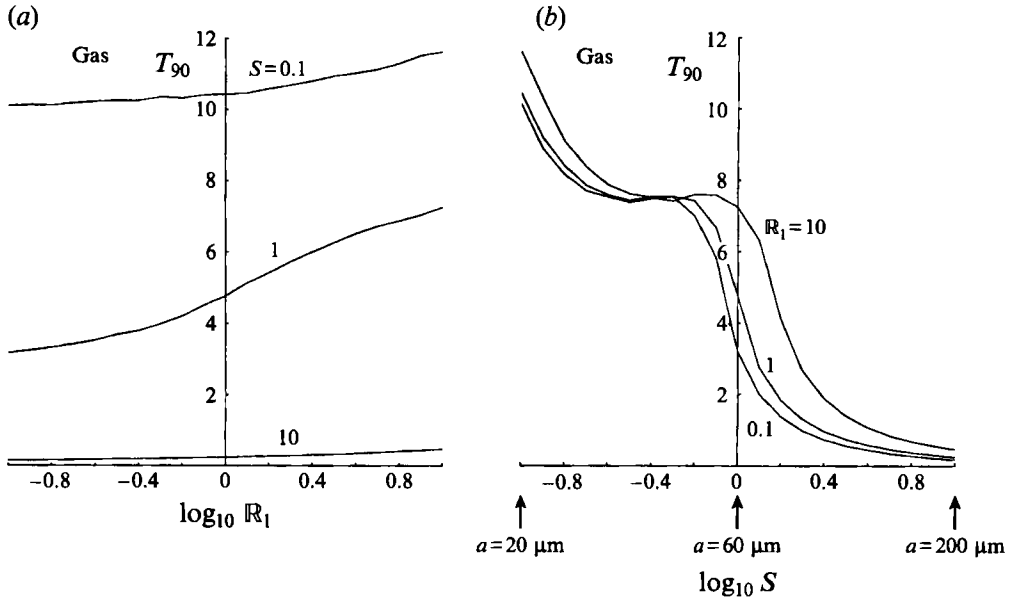

FIGURE 6. The time T_{90} within which 90% of the particles released initially at uniformly distributed points are expelled from a bubble in a gas-fluidized bed, shown (*a*) as a function of $\mathbb{R}_1$ for several values of S and (*b*) as a function of S for several values of $\mathbb{R}_1$. The values of a indicated on the abscissa refer to air as the fluidizing fluid.

Whereas particle expulsion may be attributed to centrifugal force for the smaller particles, the situation in figure 3(*d*) corresponds more to particles literally falling through the floor of the bubble under gravity. This is clearly an effective expulsion mechanism, although it raises the question: are particles prevented from raining through the roof to take their place? A possible prevention mechanism is that suggested by Clift, Grace & Weber (1974), namely, that the upper interface is stabilized by the stagnation-point motion at the bubble surface, which tends to sweep perturbations of the interface aside before they have a chance to grow. However, for our purposes it is sufficient to note, from photographs like those in figure 1, that, empirically, particles do not rain through the roof.

Although the trajectories give a good indication of the details of the particle motion, we should like to have some overall measure of the time taken by the bubble to become almost empty of particles. We have therefore calculated the paths of 10000 particles (this number being sufficient to ensure smooth statistics) initially distributed randomly with uniform probability density throughout the interior of the bubble and have ascertained the time T_{90} it takes for 90% of the particles to be expelled. Remember that the unit of time T is R/u_0, that is, the time taken by the bubble to rise through a distance of one bubble radius. Note that there exist special initial positions for which the exit time is infinite (cf. the spikes in figure 4). Nevertheless, T_{90} is a well-defined finite quantity.

T_{90} is a function of the two dimensionless parameters S (effectively a measure of particle radius) and $\mathbb{R}_1$. Figure 6(*a*) shows T_{90} as a function of $\mathbb{R}_1$ for some given values of S, and figure 6(*b*) shows the more interesting variation of T_{90} as a function of S for some given values of $\mathbb{R}_1$. The change of slope of the curves in figure 6(*b*) at values of S near 1 (or of a near 60 μm) evidently corresponds to a change of regime of the particle trajectories. At smaller values of S the particles mostly make at least one circuit before

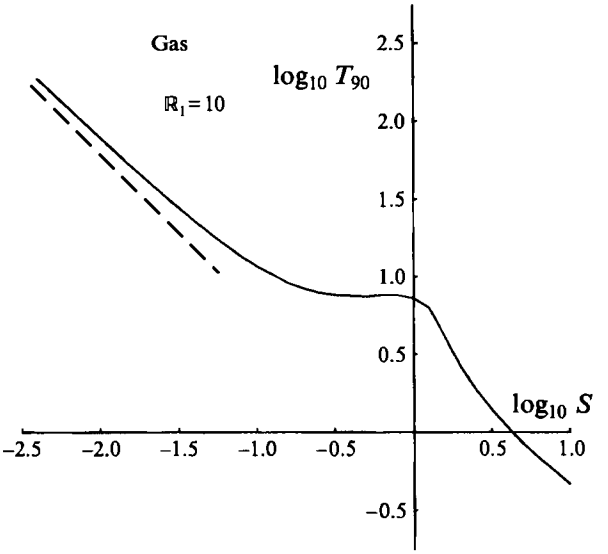

FIGURE 7. Log–log plot of T_{90} as a function of S demonstrating the asymptotic proportionality of T_{90} to S^{-1} in the limit $S \to 0$.

exiting (see figure 3), whereas at larger values of S they mostly fall through the bottom of the bubble without making a circuit.

Although exceedingly small values of S are compatible only with atypically small particle radii, it is worthwhile to extend the calculations to such values of S in order to form a link with an asymptotic relation for the limiting case where expulsion is very slow. For small S the particles follow the fluid motion closely, so that the particle acceleration is of order u_0^2/R. Moreover, the speed of fall relative to the fluid reduces to the Stokes-law value $2a^2 g\rho_p/9\mu$. These two observations imply that both inertial spiralling and gravitational settling lead to a particle velocity relative to the fluid of order S in units of u_0. This conclusion may also be reached from the dimensionless equation of motion (3.4), since the particle acceleration must approach the fluid acceleration as $S \to 0$ and this is possible only if $|V - U| = O(S)$; otherwise the last term accounting for viscous drag would become singular. The exit time starting from any initial position is thus of order S^{-1} in units of R/u_0, so that T_{90} likewise must scale as S^{-1}. Figure 7, which shows that $\log T_{90}$ becomes linear in $\log S$ with slope -1 in the limit as $S \to 0$, confirms the anticipated S^{-1} scaling and thereby provides a check on the numerical calculations.

Figure 8 shows an alternative plot, likely to be more useful in practice, of the value of T_{90} as a function of particle radius a for several different values of the particle density ρ_p and for values of μ and ρ_f appropriate to air at NTP as the fluidizing fluid. Given the particle density and fixed properties of the suspending fluid, each value of a uniquely determines the corresponding pair of parameters $(S, \mathbb{R}_1)$, and thereby the expulsion time T_{90}. As already noted, for the parameter values represented in figure 8 the minimum gas velocity for fluidization is always small compared with W, which supports our order-of-magnitude estimate (2.6) and our assumption of small cloud thickness.

It is seen from the trajectories for the larger values of a in figure 3 that the particles fall more or less vertically, their sedimentation being perturbed only a little by the circulatory fluid motion. The limiting case in which gravity dominates over viscous drag exerted by the circulatory flow is one for which the expulsion time can be

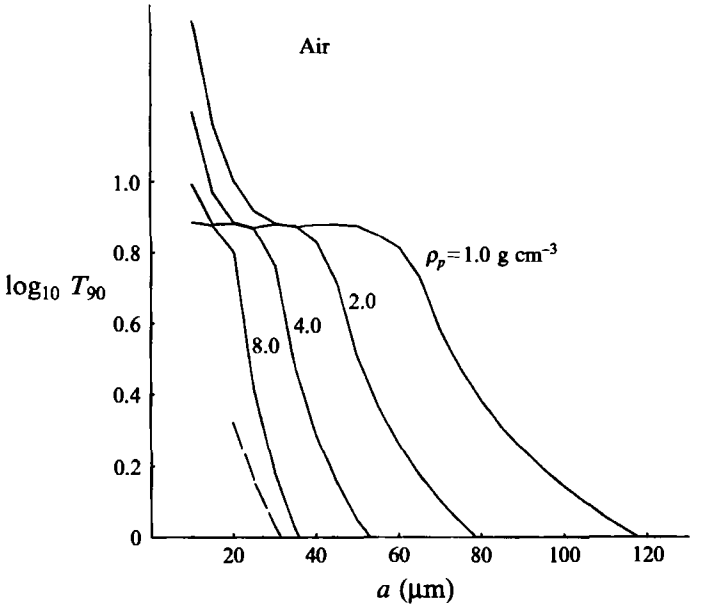

FIGURE 8. T_{90} as a function of a for several values of ρ_p; air-fluidized bed. The broken curve represents the asymptotic relation (4.2) for the case $\rho_p = 8$ g cm^{-3}.

calculated explicitly, and furnishes a further check on the numerical calculations. Since the particles start with zero initial acceleration, they fall relative to the fluid with constant terminal speed V_0 determined by the nonlinear equation

$$V_0 = \frac{2a^2 g(\rho_p - \rho_f)}{9\mu D_{V_0}} \tag{4.1}$$

representing the balance between gravitational and drag forces. The fact that all particles have the same velocity implies that the cloud is simply displaced downwards as a whole. A straightforward geometrical calculation shows that 90% of the particles have left the blob once they have collectively fallen through a distance of 1.458 times the blob radius R. Thus the expulsion time is given in units of the rise time R/u_0 by

$$T_{90} \sim \frac{1.458R}{V_0} \Big/ \frac{R}{u_0} = \frac{1.458(gR)^{1/2}}{V_0}. \tag{4.2}$$

This is the equation of the broken curve added in figure 8 for the case $\rho_p = 8$ g cm^{-3}, and it is seen to approximate the calculated values of T_{90} as the particle radius a becomes large.

The conclusion to be drawn from figure 8 is that, for even the smallest particles considered, the bubble is more or less empty after the time taken to rise through several diameters. The smaller particles take longer to be expelled.

Now that we have found that the centrifugal and gravitational forces on a particle in a buoyant compact blob are effective in expelling particles, we can suggest a reason why falling compact blobs containing particles with *above*-average concentration are not observed. The outcome of the primary and secondary instabilities of a uniform fluidized bed mentioned in §1 is likely to be the creation of compact blobs, some containing a smaller-than-average concentration of particles which rise under gravity and some a larger-than-average concentration which fall. In both cases an internal

circulation develops and centrifugal force tends to expel particles. In the case of the buoyant blobs the outcome is an empty bubble, but in the case of dense blobs the result of loss of particles due to centrifugal force is ultimately to bring the internal concentration of particles down to the same level as that in the surrounding bed. In short, bubbles are created by the expulsion of particles from a buoyant blob, but dense blobs lose their identity. There are no permanent 'anti-bubbles'.

5. The case of a liquid-fluidized bed

Having found an expulsion mechanism which could account qualitatively for the existence of particle-free bubbles in a gas-fluidized bed, we now consider whether a similar mechanism is effective in the case of a liquid-fluidized bed.

Different parameter values are relevant here. If we choose water as the typical liquid the dynamic viscosity of the fluid is now 0.010 g cm^{-1} s^{-1} at NTP, larger than that for air by a factor 55. The fluid density is no longer small in comparison with that of a particle; and when specific numerical values are under consideration we shall take

$$\rho_f = 0.998 \text{ g cm}^{-3}, \quad \rho_p/\rho_f = 1.5, 2, 4, 8.$$

Otherwise the specific values and assumptions will be the same as those for a gas-fluidized bed listed at the end of §2.

Since the fluid density is now not small, virtual-mass effects must be allowed for in the equation of motion for a particle. This is analytically feasible only if the fluid motion about each particle is irrotational, and we shall assume this to be so in the expectation that the results are not qualitatively in error. The acceleration reaction on an isolated spherical particle is then

$$-\tfrac{1}{2}m_0\left(\frac{\mathrm{d}\boldsymbol{v}}{\mathrm{d}t}-\frac{\mathrm{d}\boldsymbol{u}}{\mathrm{d}t}\right), \tag{5.1}$$

where m_0 is the mass of displaced fluid and the two time derivatives denote rates of change of the particle and fluid velocity respectively following the motion of the particle (Batchelor 1967, §6.5). The equation of motion of a particle (3.1) should thus be replaced by

$$(m+\tfrac{1}{2}m_0)\frac{\mathrm{d}\boldsymbol{v}}{\mathrm{d}t} = (m-m_0)\boldsymbol{g} - 6\pi\mu a(\boldsymbol{v}-\boldsymbol{u})D_{|\boldsymbol{v}-\boldsymbol{u}|} + \tfrac{3}{2}m_0\frac{\mathrm{d}\boldsymbol{u}}{\mathrm{d}t}. \tag{5.2}$$

Part of the last term (namely $\frac{1}{2}m_0\,\mathrm{d}\boldsymbol{u}/\mathrm{d}t$) is a consequence of (5.1) and the remaining part (namely $m_0\,\mathrm{d}\boldsymbol{u}/\mathrm{d}t$) represents the 'buoyancy' force associated with the (locally) uniform pressure gradient in the fluid that causes it to accelerate in its circulatory motion.

The particle relaxation time τ here refers to a particle moving under the action of inertia of both particle and fluid and the fluid (viscous) drag, whence

$$\tau = \frac{m+\frac{1}{2}m_0}{6\pi\mu a} = \left(1+\frac{\rho_f}{2\rho_p}\right)\tau_0. \tag{5.3}$$

If now we non-dimensionalize the equation of motion using the parameters R and u_0 as units, as in the case of a gas-fluidized bed, we obtain

$$(1+\tfrac{1}{2}\eta)\frac{\mathrm{d}\boldsymbol{V}}{\mathrm{d}T} = \frac{j(1-\eta)}{F} - \frac{\boldsymbol{V}-\boldsymbol{U}}{S}D_{|\boldsymbol{v}-\boldsymbol{u}|} + \tfrac{3}{2}\eta\frac{\mathrm{d}\boldsymbol{U}}{\mathrm{d}T}, \tag{5.4}$$

a (μm)	$\mathbb{R}_0$	$\mathbb{R}_1$	S
10	4.27×10^{-3}	8.82×10^{0}	9.82×10^{-4}
20	3.31×10^{-2}	1.76×10^{1}	3.93×10^{-3}
30	1.08×10^{-1}	2.65×10^{1}	8.84×10^{-3}
40	2.45×10^{-1}	3.53×10^{1}	1.57×10^{-2}
50	4.58×10^{-1}	4.41×10^{1}	2.46×10^{-2}
60	7.57×10^{-1}	5.29×10^{1}	3.54×10^{-2}
70	1.15×10^{0}	6.18×10^{1}	4.81×10^{-2}
80	1.63×10^{0}	7.06×10^{1}	6.29×10^{-2}
90	2.22×10^{0}	7.94×10^{1}	7.96×10^{-2}
100	2.91×10^{0}	8.82×10^{1}	9.82×10^{-2}
150	7.87×10^{0}	1.32×10^{2}	2.21×10^{-1}
200	1.53×10^{1}	1.76×10^{2}	3.93×10^{-1}
250	2.49×10^{1}	2.21×10^{2}	6.14×10^{-1}
300	3.67×10^{1}	2.65×10^{2}	8.84×10^{-1}

TABLE 2. Values of the dimensionless parameters assuming water at 20 °C to be the suspending fluid, having density $\rho_f = 0.9982$ g cm^{-3} and viscosity $\mu = 1.002 \times 10^{-2}$ g cm^{-1} s^{-1}. The particle density ρ_p is taken to be 2.0 g cm^{-3}.

where $\eta = \rho_f/\rho_p$. This general equation, for which we have developed numerical procedures, reduces to (3.4) in the limit $\rho_f/\rho_p \to 0$.

The particle trajectory depends on the dimensionless parameters

$$S = \frac{\tau_0 u_0}{R} = \frac{2a^2 g^{1/2} \rho_p}{9R^{1/2}\mu}, \quad F = \frac{u_0^2}{gR}, \tag{5.5}$$

although as before the Froude number F is always near unity for rising bubbles. In addition

$$\mathbb{R}_1 = \frac{2au_0\rho_f}{\mu} = \frac{2a(gR)^{1/2}\rho_f}{\mu} \tag{5.6}$$

is a governing parameter, as before, and finally there is the new governing parameter $\eta = \rho_f/\rho_p$.

It is clear from (5.5) that for similar values of a and R the important parameter S is much smaller for a liquid-fluidized bed in consequence of the much larger value of μ in that case. The reverse is true for the less important parameter $\mathbb{R}_1$, because ρ_f/μ for water is larger than the value for air by a factor 15. These comparisons may be seen in detail from table 1 giving values of S and $\mathbb{R}_1$ for various values of a in the case of an air-fluidized bed and the similar table 2 for a water-fluidized bed. Judging by our experience with the case of an air-fluidized bed, both the smallness of S and the largeness of $\mathbb{R}_1$ may be expected to result in a diminished tendency for particles to be thrown outward across the bubble boundary. Smallness of S is equivalent to diminished particle inertia. Largeness of $\mathbb{R}_1$ results in decreased motion of particles relative to the fluid owing to the greater drag implied by (2.3) relative to Stokes' law. Both effects cause the particles to follow the fluid more closely. There is a third reason why particle expulsion is weaker, in this case of a liquid-fluidized bed, associated with the additional term $\frac{3}{2}m_0 \mathrm{d}u/\mathrm{d}t$ in the equation of motion (5.2). This contribution to the force on a particle is everywhere directed inwards towards the centre of the nested closed streamlines of the fluid motion in a plane through the axis of symmetry, as shown in figure 9.

Note that the assumption $N/S \ll 1$ (where N is the particle mass loading $\phi\rho_p/\rho_f$) is

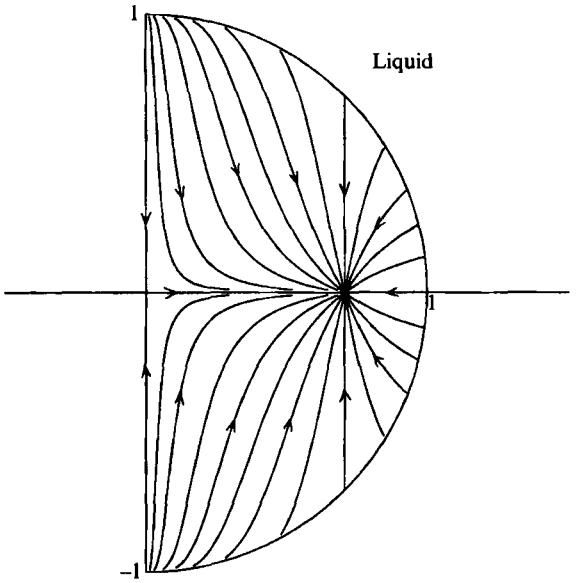

FIGURE 9. Lines everywhere parallel to the fluid acceleration $\mathrm{d}U/\mathrm{d}T$ appearing in the equation of motion (5.4).

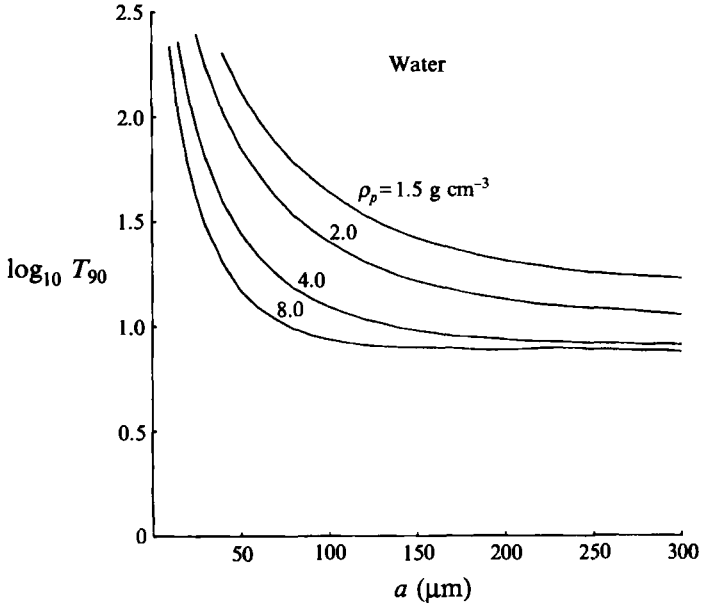

FIGURE 10. T_{90} as a function of a for several values of ρ_p; water-fluidized bed.

better satisfied here, essentially because μ/ρ_f for water is smaller than for air by a factor 1/15. Thus the fluid velocity distribution is not affected significantly by the presence of the particles, whereas in the case of the air-fluidized bed that was uncertain.

We have made numerical calculations of particle trajectories governed by the equation (5.4) like those described in §4 but with values of μ and ρ_f appropriate to water. The results for the expulsion time shown in figure 10 are qualitatively similar, but there is a big difference between the values of the exit time for the two fluidizing fluids, those for the case of water being larger. Most of the particles evidently fall

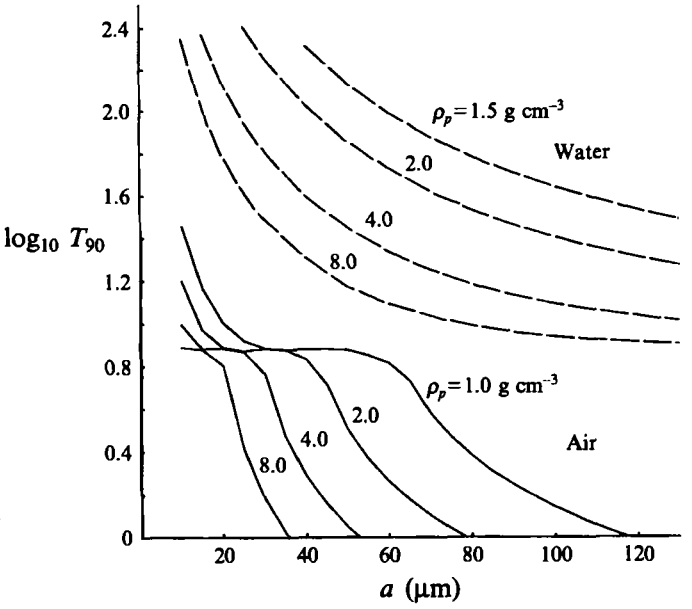

FIGURE 11. Comparison of expulsion time T_{90} as a function of particle radius a for air and water as the suspending fluid. At a given particle density ρ_p and radius a, T_{90} for the water-fluidized bed is at least ten times as large as the corresponding value for the air-fluidized bed.

through the bottom of the bubble without first making any circuit when $a > 60$ μm for $\rho_p = 1$ g cm^{-3} in the case of air as the fluidizing fluid, but similarly rapid expulsion does not occur until $a > 150$ μm with the much larger particle density $\rho_p = 8$ g cm^{-3} in the case of water. Figure 11 shows the time for 90% of 10000 particles of specified radius, initially placed randomly in the bubble, to cross the bubble boundary, for each of the two fluids. In practical terms, the expulsion mechanism is very weak for a water-fluidized bed and is unlikely to produce easily recognized effectively empty bubbles. It is thus understandable that bubbles of clear fluid have been observed in gas-fluidized beds but apparently not in liquid-fluidized beds.

6. The effect of particle interactions

It remains to make the promised attempt to estimate the effect of hydrodynamic interaction of the particles in the bubble. The attempt will be based on the empirical relation (2.4) which specifies the dependence, on both ϕ and $\mathbb{R}_0$, of the mean particle velocity V_ϕ relative to the mean volume-flux velocity of the fluid in the case of an unbounded statistically homogeneous dispersion of particles with concentration ϕ on which a steady uniform force acts.

To enable the relation (2.4) to be used we assume that:

(*a*) the particle spacing is small compared with the bubble radius and the particle dispersion is locally homogeneous within the bubble;

(*b*) the equation of mean motion of particles at a point in the bubble is of the same form as (5.2) (or its non-dimensional version (5.4)) in which v and u now stand for the local mean particle and (superficial) fluid velocity respectively;

(*c*) the mean fluid velocity in (5.2) can again be identified with the velocity distribution (2.5) appropriate to a pure fluid; and

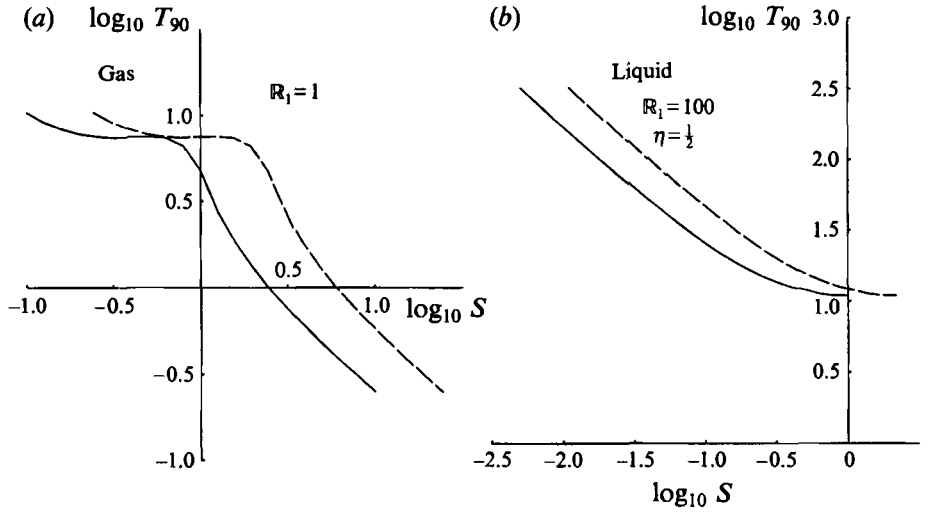

FIGURE 12. T_{90} as a function of S. The solid curves represent non-interacting particles, and the broken curves, displaced to the right from the corresponding solid curves, allow approximately for the effect of interactions at a particle concentration $\phi = 0.2$. (*a*) Parameter values representative of gas-fluidized beds; (*b*) parameter values representative of liquid-fluidized beds.

(*d*) only the second term on the right-hand side of (5.2) is affected by particle interactions.

Assumptions (*b*) and (*c*) are expedient, and (*d*) rests on the intuitive notion that the primary effect of particle interactions is to increase the resistance to motion of the particles relative to the fluid.

The meaning of (2.4) is that the average relative velocity of particles and fluid in a homogeneous dispersion with particle concentration ϕ generated by a uniform force on the particles is smaller by a factor $(1-\phi)^n$ than its value in the absence of particle interactions. It follows therefore from our assumptions that inclusion of the effect of hydrodynamic interaction of the particles leaves unchanged the non-dimensional equation of motion (5.4) except that the parameter S is replaced by

$$S_\phi = \frac{2\rho_p a^2 g^{1/2}}{9\mu R^{1/2}}(1-\phi)^n. \tag{6.1}$$

All our previous calculations of T_{90} as a function of S, $\mathbb{R}_1$ and $\eta(=\rho_f/\rho_p)$ thus remain valid when particle interactions are allowed for, provided these results for a given value of S are regarded now as applicable to the same value of S_ϕ.

Figure 11 shows that, when $\phi = 0$, T_{90} is a decreasing function of S almost everywhere, so that the effect of particle interactions is generally to increase T_{90} for both air and water as the fluidizing fluid, as expected from our assumption that the primary consequence of interactions is to increase the resistance to relative motion of the particles and the fluid. Quantitatively we allow for the effect of particle interactions simply by translating the curves T_{90} *vs.* $\log_{10} S$ along the abscissa through a 'distance' $\log_{10}(1-\phi)^{-n}$, as indicated in figure 12(*a*, *b*) for the value $\phi = 0.2$. This figure shows the effect of particle interactions through the dependence of T_{90} on S for given $\mathbb{R}_1$ (and η where applicable) over ranges of the parameters appropriate to gas (*a*) and liquid (*b*) as the suspending fluid. A slight complication is introduced by the dependence of the Richardson–Zaki exponent n on the particle Reynolds number $\mathbb{R}_0$, for in the presence

of interactions $\mathbb{R}_0$ represents a further dimensionless parameter, additional to S, $\mathbb{R}_1$ and η, that must be specified in order to determine T_{90}. In practice, as is evident from tables 1 and 2, variations of S are accompanied by variations in $\mathbb{R}_0$ (from small values to $\mathbb{R}_0 = O(10)$ for air under the conditions represented in figure 8; from small values to $\mathbb{R}_0 = O(100)$ for water under the conditions represented in figure 10). Thus the exponent n cannot strictly be regarded as constant along any of the curves. However, n depends rather weakly on $\mathbb{R}_0$ (changing by a factor less than 2 over the entire range from $\mathbb{R}_0 \to 0$ to $\mathbb{R}_0 \to \infty$), and we have elected for simplicity to use a representative value, namely $n = 4$ for gas-fluidized beds and $n = 3.5$ for liquid-fluidized beds. With these choices, figure 12 represents our rough allowance for the effects of particle interactions.

The conclusions to be drawn from this figure, and similar calculations for other values of the parameters, are that, first, for gas-fluidized beds, particle interactions can increase the expulsion time by a factor as large as about 5; however, even when interactions are allowed for, the blob becomes more or less empty within the time required for it to rise through 10 radii. Second, for liquid-fluidized beds, particle interactions can increase the expulsion time by a factor as large as about 2.

REFERENCES

BATCHELOR, G. K. 1967 *An Introduction to Fluid Dynamics.* Cambridge University Press.

BATCHELOR, G. K. 1988 A new theory of the instability of a uniform fluidized bed. *J. Fluid Mech.* **193**, 75–110.

BATCHELOR, G. K. 1991 The formation of bubbles in fluidized beds. In *Of Fluid Mechanics and Related Matters: Proc. Symp. honoring John Miles on his 70th birthday.* Scripps Inst. Oceanog. Ref. Series 91-24, pp. 29–44.

BATCHELOR, G. K. 1993 Secondary instability of a gas-fluidized bed. *J. Fluid Mech.* **257**, 359–371.

CLIFT, R., GRACE, J. R. & WEBER, M. E. 1974 Stability of bubbles in fluidized beds. *Indust. Engng Chem. Fundam.* **13**, 45–51.

DAVIDSON, J. F. & HARRISON, D. 1963 *Fluidized Particles.* Cambridge University Press.

DAVIDSON, J. F., HARRISON, D. & GUEDES DE CARVALHO, J. R. F. 1977 On the liquidlike behaviour of fluidized beds. *Ann. Rev. Fluid Mech.* **9**, 55–86.

FOSCOLO, P. U. & GIBILARO, L. G. 1984 A fully predictive criterion for the transition between particulate and aggregative fluidization. *Chem. Engng Sci.* **39**, 1667–1675.

MARBLE, F. E. 1970 Dynamics of dusty gases. *Ann. Rev. Fluid Mech.* **2**, 397–446.

MAXEY, M. R. & CORRSIN, S. 1986 Gravitational settling of aerosol particles in randomly oriented cellular flow fields. *J. Atmos. Sci.* **43**, 1112–1134.

REUTER, H. 1963 *Chem. Ing. Tech.* **35**, 98–103 and 219–228.

RICHARDSON, J. F. & ZAKI, W. N. 1954 Sedimentation and fluidization. *Trans. Inst. Chem. Engrs* **32**, 35–52.

YATES, J. G., CHEESMAN, D. J. & SERGEEV, Y. A. 1994 Experimental observations of voidage distribution around bubbles in a fluidized bed. *Chem. Engng Sci.* **49**, 1885–1895.